Thermal Management of Hybrid Silicon Ring Lasers for High Temperature Operation

Chong Zhang, Di Liang, Geza Kurczveil, John E. Bowers, Raymond G. Beausoleil

HP Laboratories
HPL-2015-40

Keyword(s):

Quantum well lasers; Ring lasers; Silicon photonics; thermal management;

Abstract:

We discuss the thermal management of microring lasers on hybrid silicon platform in order to optimize their high-temperature lasing performance. The thermal impedance of microring lasers was improved with a novel thermal shunt design. We report a significant improvement of hybrid silicon microring laser performance, with the maximum continuous wave lasing stage temperature up to 105 degC.

External Posting Date: April 21, 2015 [Fulltext] Approved for External Publication
Internal Posting Date: April 21, 2015 [Fulltext]

© Copyright 2015 Hewlett-Packard Development Company, L.P.

Thermal Management of Hybrid Silicon Ring Lasers for High Temperature Operation

Chong Zhang, *Student Member, IEEE*, Di Liang, *Senior Member*, *IEEE*, Geza Kurczveil, John E. Bowers, *Fellow, IEEE*, and Raymond G. Beausoleil, *Senior Member, IEEE*

***Abstract*—We discuss the thermal management of microring lasers on hybrid silicon platform in order to optimize their high-temperature lasing performance. The thermal impedance of microring lasers was improved with a novel thermal shunt design. We report a significant improvement of hybrid silicon microring laser performance, with the maximum continuous wave lasing stage temperature up to 105 °C.**

***Index Terms*—Quantum well lasers, Ring lasers, Silicon photonics, Thermal management**

I. Introduction

THE demand for high-speed and low-power consumption short-distance data links, especially for inter-chip communications, has led to great efforts to develop integrated photonics chips with low cost and large bandwidth. The hybrid silicon technique is a promising solution for optical interconnection applications because of its inherent advantages on integrating variety of materials with silicon-based optics through a CMOS compatible procedure [1, 2]. By transferring III-V direct-bandgap materials to silicon-on-insulator (SOI) substrate with a molecular bonding process, laser sources and many other components were developed on hybrid silicon platform, which enables variety of functions to be integrated into a single chip [3-5].

A thick low-refractive index buried oxide (BOX) layer in SOI substrate is necessary for low-substrate leakage loss waveguiding. However, the poor thermal conductivity of SiO_2 forms a barrier for heat generated in the device layer to be dissipated in the silicon substrate, which is a major obstacle for the hybrid silicon platform to achieve higher energy efficiency and higher integration density [6].

The hybrid silicon microring (HSMR) laser (Fig. 1) has a small footprint and small threshold current, which makes it a good candidate for large-scale optical interconnection application [7, 8]. However, HSMR lasers have a larger thermal impedance due to higher series resistance from the compact design. Their performance degrades rapidly with increasing input power or at rising ambient temperatures. Previous research shows a maximum CW lasing temperature at 65 °C around 1530 nm for a 50 μm diameter device [9], which limits its use in many applications.

This work was supported by the HP Labs internship research funding.

C. Zhang, D. Liang, G. Kurczveil and R. G. Beausoleil are with the Systems Research Laboratory at Hewlett-Packard Laboratories, Palo Alto, CA 94304 USA.(e-mail: czhang@ece.ucsb.edu; di.liang@hp.com; geza.kurczveil@hp.com, ray.beausoleil@hp.com).

C. Zhang and J. E. Bowers are with Department of Electrical Engineering, University of California, Santa Barbara, California 93106, USA (e-mail: czhang@ece.ucsb.edu, bowers@ece.ucsb.edu).

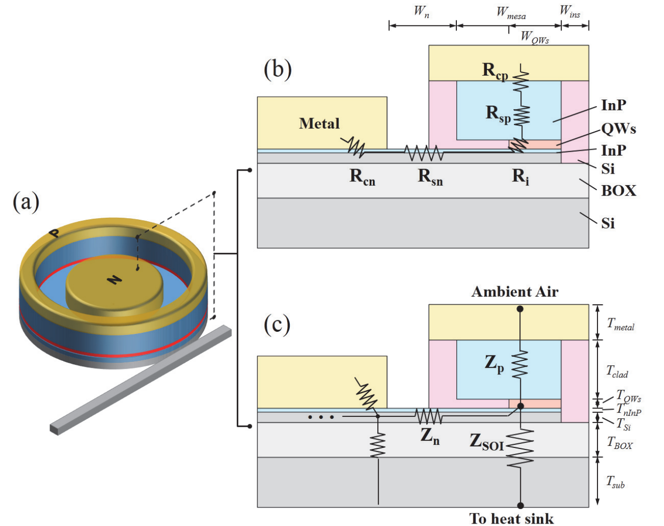

Fig. 1. (a) Diagram of a HSMR laser and schematic device cross-section with (b) electrical resistance model and (c) thermal resistance model

Efforts have been made to improve the thermal performance of HSMR lasers, for example to optimize the laser injection efficiency by undercutting the active region [9], and to reduce the device heating with a metal shunt [10]. In this paper we propose a novel thermal shunt design to improve the thermal performance of HSMR lasers. In Section II, we discuss strategies of thermal management and show the simulation results on optimization of the thermal shunt design. In Section III we will illustrate the device structure and fabrication of the HSMR lasers with double thermal shunt design. In Section IV we analyze the optical and thermal performance of devices with thermal management.

II. Thermal Analysis of Hybrid Silicon Ring Laser

When the active region temperature of quantum well (QW) lasers increases, the bimolecular recombination rate decreases and the Auger recombination rate increases [11], so the quantum efficiency of the lasers is reduced. The correlation between temperature and laser threshold can be described by

the empirical equations [12]:

$$I_{th} = I_0 e^{T/T_0} \quad (1)$$

$$\eta_d = \eta_{d0} e^{-T/T_\eta} \quad (2)$$

The above equations indicate that both the threshold current I_{th} and differential quantum efficiency η_d typically degrade exponentially with temperature, with characteristic temperatures T_0 and T_η. Both characteristic temperatures are related to thermal impedance of the device, Z_T, which is dependent on device materials, structure geometry, and the location of heat source.

The major heat source in semiconductor QW lasers is Joule heating [13]. The equivalent model of electrical resistance of cross-section of in shown in Fig. 1 (b). Table I lists the cross-section geometric dimensions of HSMR laser used in calculations and designs, as labeled in Fig. 1 (b) and (c). The total series resistance is divided into several components: contact resistance (R_{cp}, R_{cn}), cladding resistance (R_{sp}, R_{sn}), and intrinsic layer resistance (R_i). Table II lists the typical value for each component. Their contribution to the overall Joule heating can vary depends on the device geometry and doping concentration. It's noted that the n-type contact resistance and cladding resistance usually dominate, as a result of limited contact region in the center of the ring, and the small thickness of the n-InP contact layer.

Fig. 1 (c) shows the simplified impedance model from thermal prospective, in which Z_n, Z_p, and Z_{SOI} represent the thermal impedance when heat transmits through n-contact layer as well as silicon layer underneath, p-mesa and the SOI substrate with thick BOX layer, respectively. The position of heat sink relative to heat source is important here, which affects the heat flux and then the involved thermal impedance components. For normal chip placement in testing setup and device package, the heat sink is usually set underneath substrate. It turns out that the BOX layer with small thermal conductivity dominates in the overall thermal impedance of the device.

A commercial 2-D finite element modeling tool [14] was used to numerically simulated heat-transmission inside the device structures, as shown in Fig. 2. The thermal

TABLE I
CROSS-SECTION GEOMETRIC DIMENSION FOR HSMR LASER

W_{QWs}	1.5 µm	T_{QWs}	260 nm
W_{mesa}	3 µm	T_{nInP}	110 nm
W_{ins}	0.8 µm	T_{Si}	300 nm
W_n	2 µm	T_{BOX}	1 µm
T_{metal}	1 µm	T_{sub}	600 µm
T_{clad}	1.7 µm		

TABLE II
SERIES RESISTANCE COMPONENTS OF A TYPICAL HSMR LASER WITH VALUES LISTED IN TABLE I

Components		Resistance (Ω)
P	R_{cp}	2.5
	R_{sp}	2.4
Intrinsic	R_i	2.9
N	R_{cn}	3.2
	R_{sn}	3.7

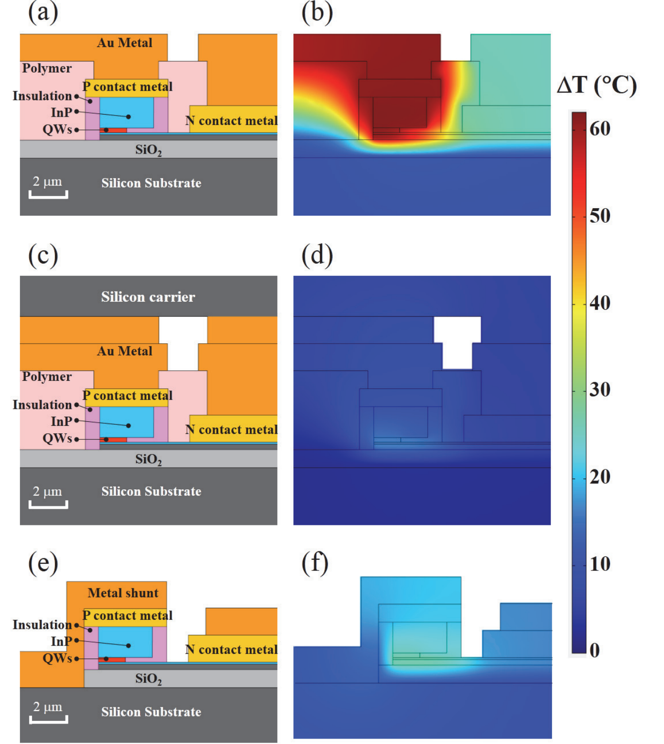

Fig. 2. Diagrams of cross-section structures of HSMR lasers and the simulated temperature contour for (a) (b) design A, (c) (d) design B, and (e) (f) design C. All results are simulated for a 50 µm diameters ring with 100 mA injection current. (b) (d) and (e) share a same temperature scale which is shown at the right side.

conductivities of materials used in a HSMR laser structure are listed in Table III. Metals normally have much larger thermal conductivity compared with most semiconductor materials. Most dielectric materials used in silicon photonics have poor thermal performance.

Three types of structures were compared in Fig. 2. They share the same active region and mesa claddings with different strategies on thermal management. A constant temperature was used as boundary condition at the bottom of silicon substrate, which represents an ideal thermal sink.

1) Design A: The standard HSMR laser structure with polymer passivation, as demonstrated in Figs. 2(a)-(b). Both polymer around the p mesa and SiO_2 in substrate

TABLE III
THERMAL CONDUCTIVITY OF SELECTIVE MATERIALS

Materials	Thermal conductivity at 20 °C W/(m·K)
Dry air	~ 0.02
Thermal SiO_2	1.38
PECVD SiN_x	1.5
Polymer (SU8, BCB)	0.3
Silicon	130
InP	68
Sapphire	27
Copper	401
Gold	318

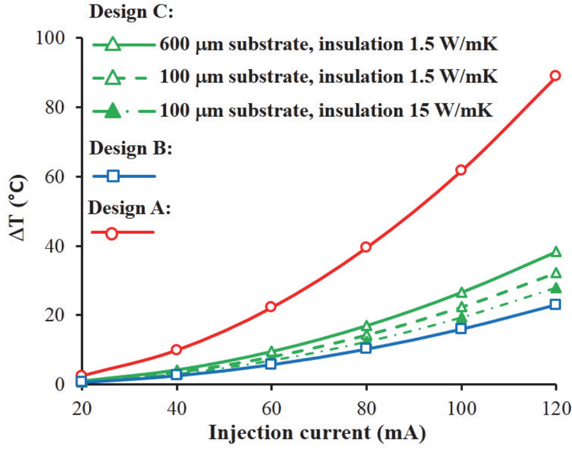

Fig. 3. Temperature changes at the laser active region with different injection current corresponding to the three structure designs shown in Fig. 2.

have poor thermal conductivity, confining the thermal energy in the limited volume of III-V materials. The active region temperature is raised by 62 ºC with 100 mA injection current.

2) Design B: A 'flip-chip bonding' design. In order to bypass the SOI substrate, the device was flip-chip bonded to a 200 μm silicon carrier wafer with the heat sink underneath, as shown in Figs. 2 (c)-(d). The p-type and n-type metal were connected to metal wires on the carrier wafer and served as the heat conduction media. The heat generated at active region dissipates into heat sink through the p-mesa into carrier wafer efficiently and the active region stays cool.
3) Design C: A 'p-metal thermal shunt' design, as shown in Fig. 2 (e) (f). The 1 μm BOX layer was etched through with metal filled in. Thick metal covers the entire III-V mesa including the steep sidewall, efficiently "shorting" the heat from active region, p-mesa all the way to the silicon substrate.

Thick SiN_x was used as dielectric layer to isolate the active region with metal to avoid a large absorption loss. The simulation results indicate an effective heat transmission between heat source and heat sink with the maximum temperature at the active region much lower than design A.

The active region temperature for all three designs are shown in Fig. 3. Design A has the worst thermal performance. The overall impedances for each design with 50 μm diameter are 420 °C/W, 109 °C/W and 181 °C/W, respectively.

The flip-chip bonding approach has the best cooling efficiency. But it normally requires high-precision position alignment and is incompatible with integration with electronics and external optical fibers. The difficulties in process and package make it less desirable.

It is worthwhile to note that further optimization can be done by tuning the device structures. As shown in the plots in Fig. 3, a thinner SOI substrate (100 μm) improves the thermal impedance by 16% compared with a 600 μm substrate [15]. An additional 12% improvement could be achieved by improving the thermal conductivity of insulation layers from 1.5 W/(m·K) to 15 W/(m·K), although the availability of these materials in our fabrication facilities were limited in this work.

In addition, the above simulations were based on a simplified model that neglects the boundary thermal resistance. The multiple layer system in practice has more complex heat transmissions and larger thermal impedance, depending on the surface treatment process as well as the deposition techniques.

III. Device Design and Fabrication

There are two aspects to optimize the thermal performance of a HSMR laser based on the previous discussion: heat sources and heat-flux path. The former requires improving the injection efficiency and the device series resistance; the latter requires optimization of the metal thermal shunt design. A double thermal-shunt structure is investigated here to improve the previous design [10] (Fig. 4 (a)). A p-metal thermal shunt with

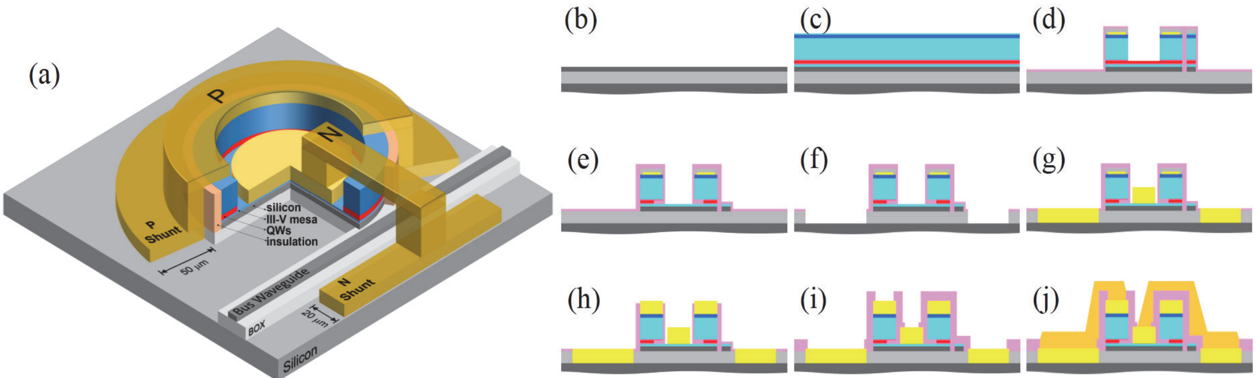

Fig. 4. (a) The diagram of a HSMR laser with double thermal shunt design. (b) to (j) illustrate the hybrid silicon process flow: (b) waveguide and other passive components were etched on SOI substrate; (c) III-V film with active region was bonded onto SOI substrate; (d) Ring mesa was defined by dry etches; (e) active region was undercuted by wet etches; (f) BOX layer was etched through with dry etching method; (g) n-contact metal deposition; (h) p-contact metal deposition; (i) device was passivated by thick dielectric materials deposition and via openings were etched; (j) Shunt metal as well as probe metals were deposited.

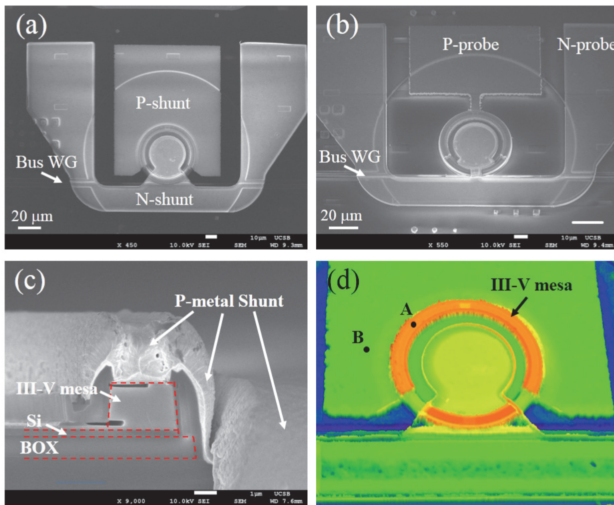

Fig. 5. plain-view SEM images of (a) HSMR lasers with double thermal shunt design and (b) control design without thermal shunt; (c) cross-section SEM image of the laser mesa with highlighted metal shunt coverage at the mesa sidewall; (d) 3-D microscopic image of the fabricated devices. The height contrast between the mesa top (spot A) and p metal shunt (spot B) is about 3.2 µm. Devices shown above are with 50 µm diameter.

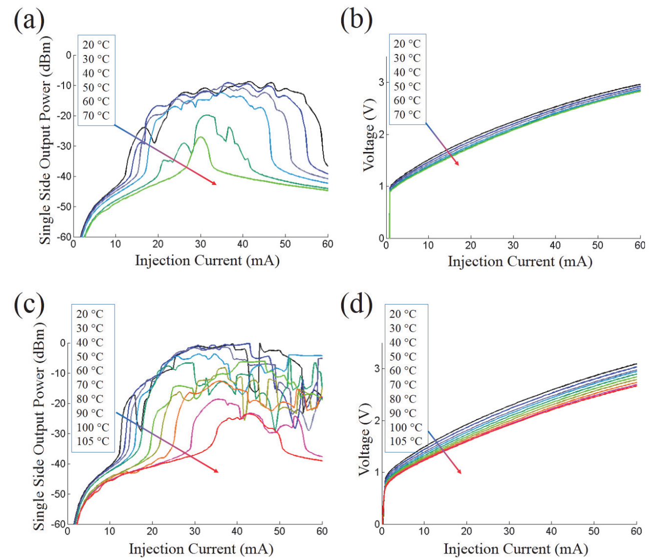

Fig. 6. (a) L-I curves and (b) I-V curves of 50 µm diameter HSMR laser without thermal shunts at different stage temperatures; (c) L-I curves and (d) I-V curves of HSMR laser with same geometry as well as double thermal shunts at different stage temperatures.

50 µm width was connected with the ring mesa. The n-metal thermal shunt with a 20 µm width was connected to the n–metal across the bus waveguide. 1 µm dielectric layer was used to insulate the p-shunt and mesa as well as between the n-shunt and p-contact. Gold was used for metal shunts in this experiment.

The active region of the III-V ring mesa includes five InAlGaAs QWs with center photoluminescence peak at 1310 nm. Compressive strain in the QW layer was used to further decrease internal loss in cavity and increase the differential gain.

HSMR lasers with diameter of 20 µm, 30 µm and 50 µm were fabricated with the hybrid silicon process using the process flow shown in Figs. 4 (b)-(j). A low temperature hydrophilic bonding technique was used to transfer III-V thin layer with gain materials to a patterned SOI substrate [16]. No precise position alignment was required for the wafer bonding process. A standard top-down III-V process was followed to fabricate mesa structure with metal electrodes deposited. As the last step of the process, the SOI substrates were thinned down to 150 µm.

Fig. 5 shows the plain-view scanning electron microscope (SEM) and optical microscope images of the fabricated HSMR lasers with thermal shunts highlighted. A control design without thermal shunt structure was processed on same wafer in parallel, as shown in Fig. 5 (b), for which the mesa structures were same except the BOX layer was left un-etched. Fig. 5 (c) shows the cross-section SEM image of the ring mesa with thermal shunt design. It shows that the 3 µm thick p-metal shunt fully covers the entire mesa with a top to sidewall thickness ratio of 3:1. 1 µm SiO_2 served as the insulation layer between the shunt and active region. It also shows the 700 nm undercut at the active region to increase the injection efficiency. But the undercut is not uniform inside the ring due to an anisotropic wet etch. Fig. 5 (d) shows the 3-D view of the device with the large height contrast from margin area with the mesa top that was capped by thick metal.

IV. Hybrid Silicon Microring Lasers Performance

The fabricated chips were placed p-side up on a copper heat

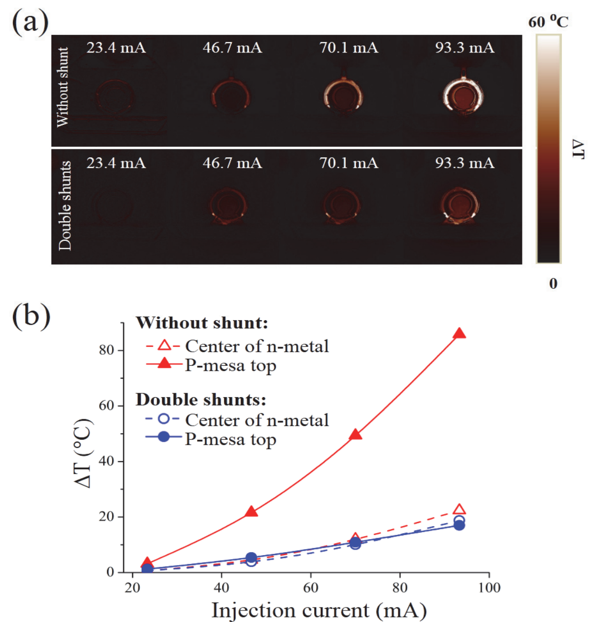

Fig. 7. (a) Thermal reflection images of 50 mm HSMR lasers with and without thermal shunt designs which show the temperature increment and distributions with different injection current. (b) The temperature changes at the monitoring spots on the devices.

sink with temperature stabilized by a thermoelectric cooler. The output light from one side of the bus waveguide was coupled into a cleaved fiber through vertical grating couplers, while the output from the other side was collected by the on-chip photodetectors. A calibrated external InGaAs photo-detector was used to detect the output power from the grating coupler and optical spectrum analyzer was used to detect the light spectrum.

Fig. 6 compares the light-current (L-I) and current-voltage (I-V) curves of HSMR lasers with and without thermal shunt designs, corresponding to the devices shown in Fig. 5 (a) and (b), respectively. From the I-V curves it was seen that the series resistance of the devices were not affected by thermal shunts design, which implies an equivalent heat source for both structures. When the stage temperature was at 20 °C, both devices shared the same threshold current around 12.3 mA. The device without thermal shunt had earlier thermal roll-over in the output power, and its maximum CW lasing temperature was about 70 °C. The device with double thermal shunts, in contrast, was able to CW lase up to 105 °C. The L-I curves show a slower thermal roll-over at same stage temperature with the output power 8 to 10 dB higher.

A thermal reflection technique [17] was used to measure the temperature at the device surface. Fig. 7 (a) shows the thermal reflection images and temperature increment with injection current on the same devices shown in Fig. 6. It shows that the 50 μm HSMR laser without thermal shunt had rapid temperature increase with increasing injection currents. The

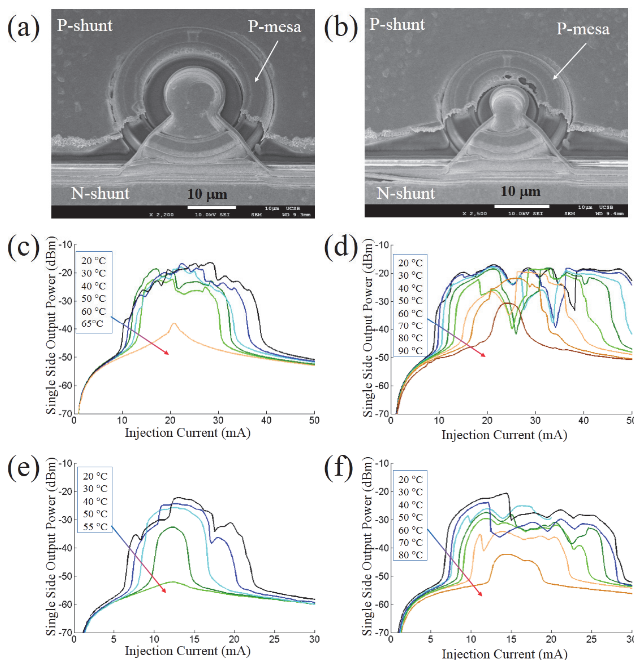

Fig. 8. Plain-view SEM images of HSMR lasers with (a) 30 μm and (b) 20 μm diameters with thermal shunts. (c) L-I curves of 30 μm control design without thermal shunt and corresponding (d) thermal shunt design; (e) L-I curves of 20 μm control design without thermal shunt and corresponding (f) thermal shunt design.

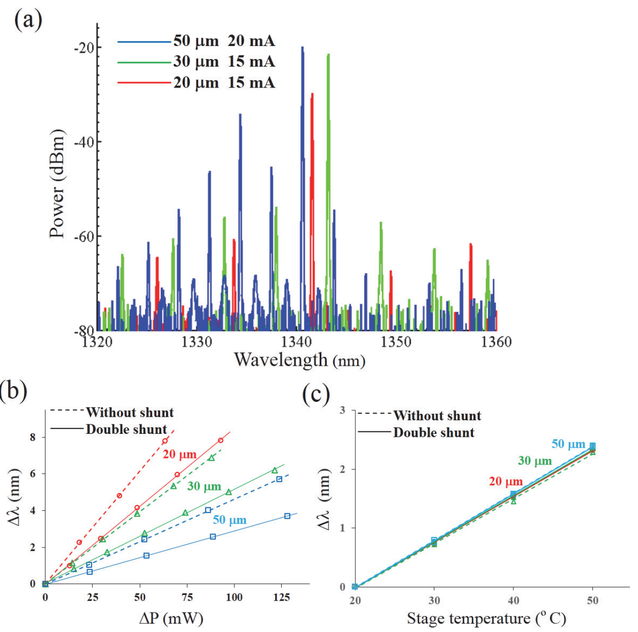

Fig. 9. (a) The spectra of HSMR lasers with thermal shunts. (b) Wavelength shift with injection power increment for HSMR lasers with different diameters. (c) Wavelength shift with stage temperature for HSMR lasers with different diameters.

heating was concentrated at the top of the ring mesa. The temperature change on the device with double thermal shunts was much less significant, with the heat spread into neighboring shunt regions. This gives clear evidence on the improvement of device thermal impedance by the thermal shunts designs.

Temperature monitoring spots were chosen at p-mesa top and center of the n-metal pads, with the temperature evolution curves shown in Fig. 7 (b). The trend of the temperature curves matches well with the simulation results in Fig. 3. For the device without a thermal shunt, the big temperature contrast between p-mesa and n-metal indicates ineffective heat transmission mesa through the thin n-contact layer and silicon device layer. With the same injection current at 93 mA, the temperature at the p mesa top at the device with double thermal shunts was 17 °C, about 65 °C lower than that of the control design. The large temperature difference provides clear evidence on the improvement of thermal impedance by the effective heat transmission by thermal shunts.

The thermal performance of HSMR lasers with smaller size was also investigated. The total series resistance of device increases with smaller device geometry. SEM images of double thermal shunt HSMR laser with a 30 μm and 20 μm diameters were shown in Figs. 8 (a) and (b), respectively. The p-metal shunt coverage was limited by size of the ring as well as the position of bus waveguide. Similarly, the respective lasing characteristic of the devices were compared in Figs. 8 (c) to (f). Smaller HSMR lasers had lower output power roll-over compared with the 50 μm ones. Notable improvements on the output power as well as lasing temperature were observed with the thermal shunt design.

TABLE IV
PERFORMANCE OF HSMR LASES WITH OR WITHOUT THERMAL SHUNT

	Diameter (μm)	Maximum CW Temperature (°C)	$d\lambda/dP$ (nm/W)	Z_T (°C/W)
Without shunt	50	70	46.3	579.9
	30	60	78.4	1031.3
	20	50	122.5	1591.1
Double shunt	50	105	29.0	363.9
	30	90	51.3	653.2
	20	80	85.1	1105.1

Fig. 9 (a) shows the spectra of HSMR lasers with thermal shunts. The free spectral range for 50 μm, 30 μm and 20 μm ring diameters were 3.11 nm, 5.18 nm and 7.81 nm, respectively. The CW output light wavelength shift with dissipation power and stage temperature of the HSMR lasers were studied, as shown in Fig. 9 (b) and (c). The temperature changes at the active region with self-heating by injected electrical power were shown in Fig. 9 (b). The slope of the fitting lines is listed in Table IV. By ignoring the 1.2% change on series resistance for 10 °C temperature difference, the self-heating was assumed to be constant, and the wavelength shifts with stage temperature were independent on the size of ring and the thermal shunt designs, as shown in Fig. 9 (c).

Then the thermal impedance of the HSMR lasers can be calculated with followed equation:

$$Z_T = \frac{d\lambda}{dP} \bigg/ \frac{d\lambda}{dT} \quad (3)$$

The calculated thermal impedance values for the devices with and without thermal shunt with varying diameters were listed in table III. As can be seen that 30% to 40% improvement in thermal impedance was achieved on the devices with thermal shunts, with the maximum CW lasing temperatures raised by over 35 °C.

V. CONCLUSION

In this paper we compared strategies to optimize the thermal management for HMSR lasers. We proposed novel double thermal shunts designs that effectively improve the thermal impedance of the device as well as the overall performance. The experimental results show that a compact HSMR laser with 50 μm diameter achieved a maximum lasing temperature at 105 °C, which matches the record of lasers on the hybrid silicon platform [18]. This is important for HSMR lasers to be used in interconnection applications in un-cooled environment, such as data centers. Further improvement could be done by using metals with higher thermal conductivity, such as copper, which is also CMOS process compatible, to optimize the efficiency of the thermal shunts.

ACKNOWLEDGMENT

Authors would like to thank Rachel Koltun, Michael L. Davenport, Jared C. Hulme and Sudharsanan Srinivasan for useful discussion and comments and acknowledge the NNIN fabrication facility at the University of California, Santa Barbara for process support.

REFERENCES

[1] A.W. Fang, H. Park, R. Jones, O. Cohen, M. J. Paniccia, and J. E. Bowers, “A continuous-wave hybrid AlGaInAs-silicon evanescent laser,” *IEEE Photon. Technol. Lett.,* vol. 18, no. 10, pp. 1143–1145, May 2006

[2] M. J. R. Heck, J. F. Bauters, M. L. Davenport, J. K. Doylend, S. Jain, G. Kurczveil, S. Srinivasan, Y. Tang, and J. E. Bowers, “Hybrid silicon photonic integrated circuit technology,” *IEEE J. Sel. Topics Quantum Electron.,* vol. 19, no. 4, p. 6100117, Jul./Aug. 2013.

[3] M. N. Sysak, J. O. Anthes, J. E. Bowers, O. Raday, and R. Jones, “Integration of hybrid silicon lasers and electroabsorption modulators,” *Opt.Exp.,* vol. 16, pp. 12478–12486, 2008.

[4] C. Zhang, S. Srinivasan, Y. Tang, M. JR Heck, M. L. Davenport, and J. E. Bowers. "Low threshold and high speed short cavity distributed feedback hybrid silicon lasers." *Opt.Exp.,* vol. 22, pp. 10202-10209. 2014.

[5] S. R. Jain, Y. Tang, H-W Chen, M. N. Sysak, and J. E. Bowers, "Integrated Hybrid Silicon Transmitters," *J. Lightwave Technol.,* 30(5), 671-678 (2012).

[6] M. N. Sysak, D. Liang, M. Fiorentino, R. G. Beausoleil, G. Kurceival, M. Piels, R. Jones, and J. E. Bowers, “Hybrid silicon evanescent laser technology: A thermal perspective,” *IEEE J. Sel. Topics Quantum Electron.,* 17, 1490-1498 (2011)

[7] D. Liang, M. Fiorentino, T. Okumura, H.-H. Chang, D. Spencer, Y.-H.Kuo, A.W. Fang, D. Dai, R. G. Beausoleil, and J. E. Bowers, “Electrically pumped compact hybrid silicon microring lasers for optical nterconnects,” *Opt. Exp.,* vol. 17, pp. 20355–20364, Sep. 20–24, 2009.

[8] D. Liang, M. Fiorentino, R. G. Beausoleil, and J. E. Bowers, “Low threshold hybrid silicon microring resonator lasers,” in *IEEE/LEOSWinter Topical Meeting.* Majorca, Spain, 2010, Paper TuD4.

[9] D. Liang, M. Fiorentino, S. Srinivasan, J. E. Bowers, and R. G. Beausoleil, “Low threshold electrically-pumped hybrid silicon microring lasers,” *IEEE J. Sel. Topics Quantum Electron.,* vol. 17, no. 6, pp. 1528–1533, Nov./Dec. 2011.

[10] D. Liang, S. Srinivasan, M. Fiorentino, G. Kurceival, J. E. Bowers, and R. G. Beausoleil, “A Metal Thermal Shunt Design for Hybrid Silicon Microring Laser,” in *IEEE Optical Interconnects Conference*, Santa Fe, USA, 2012, TuD2

[11] T. J. Houle, J. C. L Yong, C. M. Marinelli, S. Yu, J. M. Rorison, J. H. White, J. K. White, A. J. Spring Thorpe, and B. Garret, “Characterization of the temperature sensitivity of gain and recombination mechanisms in 1.3 μm AlGaInAs MQW lasers,” *IEEE J. Sel. Top. Quantum Electron.* vol. 41, no. 2, pp. 132–139, Feb. 2005.

[12] L. A. Coldren and S. W. Corzine, *Diode Lasers and Photonic Integrated Circuits*. New York: Wiley-Interscience, 1995.

[13] G. P. Agrawal and N. K. Dutta, Semiconductor Lasers. New York: Van Nostrand Reinhold, 1993.

[14] http://www.comsol.com/

[15] D. Liang, M. Fiorentino, S. T. Todd, G. Kurczveil, R. G. Beausoleil, and J. E. Bowers, “Fabrication of silicon-on-diamond substrate and low-loss optical waveguides,” *IEEE Photon. Technol. Lett.,* vol. 23, no. 10, pp. 657–659, May 2011.

[16] D. Liang and J. E. Bowers, “Highly efficient vertical outgassing channels for low-temperature InP-to-silicon direct wafer bonding on the silicon- on insulator substrate,” *J. Vac. Sci. Technol. B*, vol. 26, no. 4, pp. 1560–1568, Jul. 1, 2008.

[17] P. M. Mayer, D. Lüerßen, R. J. Ram, and J. A. Hudgings, “Theoretical and experimental investigation of the thermal resolution and dynamic range of CCD-based thermoreflectance imaging”, *J. Opt. Soc. Am. A*, vol. 24, no. 4, pp. 1156-116, Apr. 2007.

[18] H.-H. Chang, A. W. Fang, M. N. Sysak, H. Park, R. Jones, O. Cohen,O. Raday, M. J. Paniccia, and J.E. Bowers, “1310 nm Silicon Evanescent Laser,” *in Proc. 4th IEEE Int. Conf. Group IV Photon.,* Sep. 19–21, 2007, pp. 1–3.

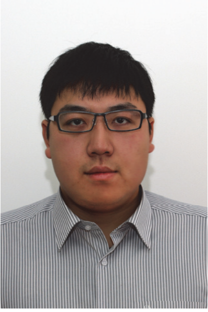

Chong Zhang (S'13) received the B.S. degree in electrical science and technology from the Harbin Institute of Technology, Harbin, China, in 2007, and the M.S. degree in optical engineering from Zhejiang University, Hangzhou, China, in 2010. He is currently working toward the Ph.D. degree at the University of California, Santa Barbara, CA, USA. His research interests include epitaxial growth of III/V materials on silicon, photonics integration devices on hybrid Silicon platform and applications for high speed optical interconnection. He worked with HP Labs (Palo Alto, CA) from Jun. to Dec. 2014 with research focus on high performance hybrid silicon microring lasers.

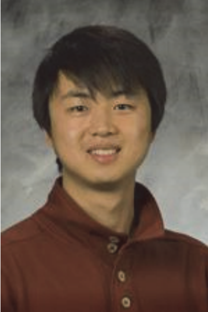

Di Liang (S'02–M'07–SM'14) is currently a research scientist at HP Labs (Palo Alto, CA). He received his B.S. degree in Optical Engineering from the Zhejiang University, Hangzhou, China in 2002, and his M.S. and Ph.D. degrees in Electrical Engineering from the University of Notre Dame, Indiana, USA in 2004 and 2006, respectively. His research interests include III-V and silicon photonics, hybrid integration and nanofabrication technology. He has authored and coauthored over 120 journal and conference papers, three book chapters.

Geza Kurczveil received the B.S. degree in physics from the University of California, Santa Cruz, in 2006 and the M.S. and Ph.D. degrees in electrical and computer engineering from the University of California Santa Barbara, Santa Barbara, in 2009 and 2012, respectively. Currently he is a research scientist at HP Labs, Palo Alto, CA. His research interests include silicon photonic integrated circuits.

John E. Bowers (F'93) holds the Fred Kavli Chair in Nanotechnology, and is the Director of the Institute for Energy Efficiency and a Professor in the Departments of Electrical and Computer Engineering and Materials at UCSB. He is a cofounder of Aurrion, Aerius Photonics and Calient Networks. Dr. Bowers received his M.S. and Ph.D. degrees from Stanford University and worked for AT&T Bell Laboratories and Honeywell before joining UC Santa Barbara. Dr. Bowers is a member of the National Academy of Engineering and a fellow of the IEEE, OSA and the American Physical Society. He is a recipient of the OSA/IEEE Tyndall Award, the OSA Holonyak Prize, the IEEE LEOS William Streifer Award and the South Coast Business and Technology Entrepreneur of the Year Award. He and coworkers received the EE Times Annual Creativity in Electronics (ACE) Award for Most Promising Technology for the hybrid silicon laser in 2007.

Bowers' research is primarily in optoelectronics and photonic integrated circuits. He has published ten book chapters, 600 journal papers, 900 conference papers and has received 54 patents. He has published 180 invited papers and conference papers, and given 16 plenary talks at conferences.

Raymond G. Beausoleil (S'86–M'86–SM'06) received the B.S. degree from Caltech, Pasadena, CA, USA, in 1980, and the Ph.D. degree from Stanford University, Stanford, CA, in 1986, both in physics. He is currently an HP Fellow in the Systems Research Laboratory at HP Laboratories, Palo Alto, CA, where he leads the Large-Scale Integrated Photonics Research Group. Prior to HP, his research was focused on high-power all-solid-state laser and nonlinear optical systems, as well as numerical algorithms for computer firmware (leading to the navigation algorithms for the optical mouse). At HP Labs, he performs basic research in microscale and nanoscale integrated photonic technologies for classical and quantum information processing. He is a Consulting Professor of Applied Physics at Stanford University, where he conducts research on quantum optics and models laser interferometric gravitational-wave interferometers. He has contributed to more than 350 papers and conference proceedings (including many invited papers and plenary/keynote addresses) and five book chapters. He has more than 105 patents issued, and more than four dozen pending. He is a Fellow of the American Physical Society.